The Astrophysical Journal, 740:19 (7pp), 2011 October 10 doi:10.1088/0004-637X/740/1/19

EVOLUTION OF CURRENTS OF OPPOSITE SIGNS IN THE FLARE-PRODUCTIVE SOLAR ACTIVE REGION NOAA 10930

B. Ravindra[1], P. Venkatakrishnan[2], Sanjiv Kumar Tiwari[2,3], and R. Bhattacharyya[2]
[1] Indian Institute of Astrophysics, Koramangala, Bangalore 560 034, India; ravindra@iiap.res.in
[2] Udaipur Solar Observatory, Physical Research Laboratory, Dewali, Bari Road, Udaipur 313 001, India; pvk@prl.res.in, tiwari@mps.mpg.de, ramit@prl.res.in
[3] Max-Planck-Institut für Sonnensystemforschung, 37191 Katlenburg-Lindau, Germany
Received 2011 April 18; accepted 2011 July 11; published 2011 September 21

ABSTRACT

Analysis of a time series of high spatial resolution vector magnetograms of the active region NOAA 10930 available from the Solar Optical Telescope SpectroPolarimeter on board *Hinode* revealed that there is a mixture of upward and downward currents in the two footpoints of an emerging flux rope. The flux emergence rate is almost the same in both the polarities. We observe that along with an increase in magnetic flux, the net current in each polarity increases initially for about three days after which it decreases. This net current is characterized by having exactly opposite signs in each polarity while its magnitude remains almost the same most of the time. The decrease of the net current in both the polarities is due to the increase of current having a sign opposite to that of the net current. The dominant current, with the same sign as the net current, is seen to increase first and then decreases during the major X-class flares. Evolution of non-dominant current appears to be a necessary condition for flare initiation. The above observations can be plausibly explained in terms of the superposition of two different force-free states resulting in a non-zero Lorentz force in the corona. This Lorentz force then pushes the coronal plasma and might facilitate the magnetic reconnection required for flares. Also, the evolution of the net current is found to follow the evolution of magnetic shear at the polarity inversion line.

Key words: Sun: evolution – Sun: flares – sunspots

1. INTRODUCTION

The magnetic field in sunspots has been studied with increasing details ever since Hale's first detection (Hale 1908). With the advent of vector magnetographs, it is now possible to estimate a few components of the competing electrodynamic forces (Borrero et al. 2008; Venkatakrishnan & Tiwari 2010), which had been invoked to define the sunspot structure and equilibrium (Chitre 1963; Meyer et al. 1977; Parker 1979; Low 1984). An important electrodynamic quantity in this context is the electric current, which is expected to play a crucial role in eruptive processes (Melrose 1991; Longcope & Welsch 2000). Such currents in astrophysical plasmas are generally produced by deforming magnetic fields through the motion of the plasmas in which the fields are embedded (Parker 1979). The sites of these deformations could be either the convection zone (Fan 2009; Longcope et al. 1998) with subsequent emergence of the deformed fields (Leka et al. 1996) or the photosphere (Aulanier et al. 2005).

A classic case of flux emergence was seen in the active region (AR) NOAA 10930, which has been well studied for a variety of flare-related magnetic phenomena. Although the emergence of current-carrying fine structures has been reported (Lim et al. 2010; Wang et al. 2008), there has so far been no study of the evolution of the net current in this region. Such a study is important because of the highly flare-productive nature of this active region. In this paper, we follow the time evolution of the net vertical current in the whole active region spanning two major X-class flares and show some new properties of current-bearing flux emergence that seem to be relevant for the triggering of the flares.

2. OBSERVATIONAL DATA AND ITS PROCESSING

The SpectroPolarimeter (Tsuneta et al. 2008; Suematsu et al. 2008; Ichimoto et al. 2008) on board *Hinode* (Kosugi et al. 2007) makes spectropolarimetric measurements at a spatial sampling of 0.″3. The I, Q, U, and V Stokes profiles have been obtained in 6301.5 Å and 6302.5 Å lines. The spectropolarimeter makes the maps of the Stokes vector by scanning the slit across the active regions. The spatial sampling is 0.″295 pixel^{-1} along the slit direction and 0.″317 pixel^{-1} in the scanning direction. There are many modes of observations depending on the exposure time, resolution, signal-to-noise ratio, etc. We have obtained the data of AR NOAA 10930 in the fast mapping mode. The Stokes signals are calibrated using the standard solar software pipeline for the spectropolarimetry. The complete information on the vector magnetic fields is obtained by inverting the Stokes vector using the Milne–Eddington inversion (Skumanich & Lites 1987; Lites & Skumanich 1990; Lites et al. 1993). The ambiguity in the transverse field is resolved based on the minimum energy algorithm developed by Metcalf (1994) and implemented in FORTRAN by Leka et al. (2009). The magnetic field vector has been transformed to the disk center using the method described by Venkatakrishnan et al. (1989). The resulting vertical (B_z) and transverse (B_t) magnetic fields have measurement errors of 8 G and 23 G, respectively.

The horizontal components of the magnetic fields B_x and B_y are utilized in computing the vertical current density J_z as

$$J_z = \frac{1}{\mu}\left(\frac{\partial B_y}{\partial x} - \frac{\partial B_x}{\partial y}\right), \quad (1)$$

where μ is the magnetic permeability.

We computed the net current in the active region separately for the N- and S-polarity regions by integrating the current density over the surface. This has been done only for those pixels whose B_z values are larger than 50 G to avoid noisy pixels and pixels that do not belong to the active region.

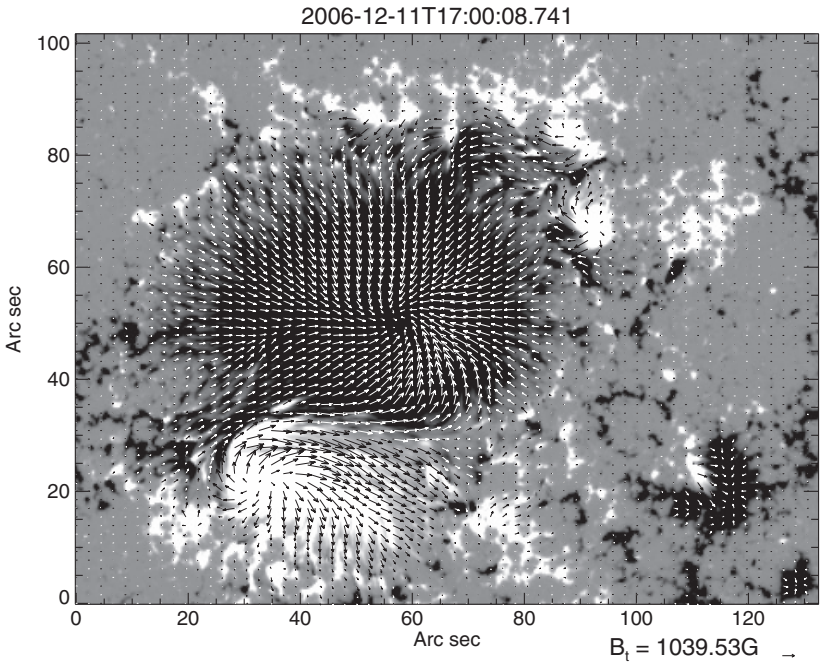

Figure 1. Sample vector magnetogram showing the ambiguity-resolved transverse field overlaid on the vertical magnetic field. The black (white) color represents the S (N) polarity regions. Arrows indicate the direction of the transverse magnetic fields.

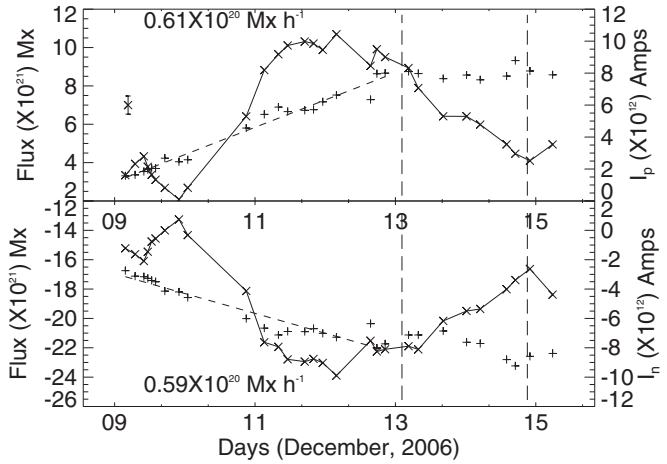

Figure 2. Evolution of flux (+ symbols) in north (top) and south (bottom) polarities is plotted as a function of time. The small dashed lines represent the linear least-squares fit to the data points. The net vertical current (× symbols) in each of these polarities is shown in the same plot. The negative (positive) net vertical current is observed in the north (south) polarity spot. The *Y*-axis on the right side shows the net currents. The long vertical lines represent the onset time of X3.4- and X1.3-class flares. The × symbol with a vertical bar shown on the top plot in the left-hand side is the error in measuring the net current.

3. RESULTS

Figure 1 shows a sample vector magnetogram of AR NOAA 10930. Both N-polarity and S-polarity sunspots are present in the active region. The S-polarity sunspot is large and well developed. The N-polarity sunspot is small and emerging. The transverse field vectors are highly sheared near the polarity inversion lines (PIL). Figure 2 shows the temporal evolution of magnetic flux in N- and S-polarity regions for six days. The flux has been estimated for those pixels whose vertical magnetic field strength is larger than 50 G. The flux is observed to increase from the beginning of the observations until the end of December 12, and thereafter no flux emergence is seen up to the middle of December 14. This is followed by a small flux emergence before the X1.3-class flare followed by a decrease in flux. Since we have used the pixels where B_z values are larger than six times the measurement error, the error in flux computation is negligible. The flux increased linearly from December 9 until the end of December 12 at a rate of about 0.6×10^{20} Mx hr^{-1} in both polarities. This indicates the emergence of a flux rope with end points in the N and S polarities of this active region.

3.1. Spatial Map of Vertical Current Density

Figure 3 shows the spatial maps of vertical current densities at different epochs. The figure also shows how the distribution of current densities in spatial locations evolves over time. The current density is of mixed sign (salt and pepper) in the umbra of the S-polarity sunspot, while it is in the form of fibrils in the penumbra, alternatively changing their sign azimuthally, as has been reported by Su et al. (2009) and Tiwari et al. (2009). Apart from these, there is a region of dominant sign of current density in the S- and N-polarity regions. In the S-polarity region, the positive current density is dominant and in the N-polarity region the negative current density is dominant. These regions are shown by arrows in both polarities (Figure 3, bottom left). These dominant regions grow with time. They occupy a portion of the umbra and also extend to the penumbra in both polarities. The vertical current density is distributed over a wide range of magnitudes. Figure 4 shows the histogram of the vertical current density in the active region. The figure shows that positive as well as negative current densities exist in the active region and its tail is extended up to ± 200 mA m^{-2}. The amplitude of variation of the vertical current density on small scales is comparable to that seen in the less flare-productive region 10933 by Venkatakrishnan & Tiwari (2009).[4]

[4] Erratum for Venkatakrishnan & Tiwari (2009): the left panel of Figure 4 in Venkatakrishnan & Tiwari (2009) shows a vertical current density map of NOAA AR 10933 with the magnitudes ranging between ± 30 mA m^{-2} which were inadvertently given as giga-amperes per square meter in the caption and also once in the text.

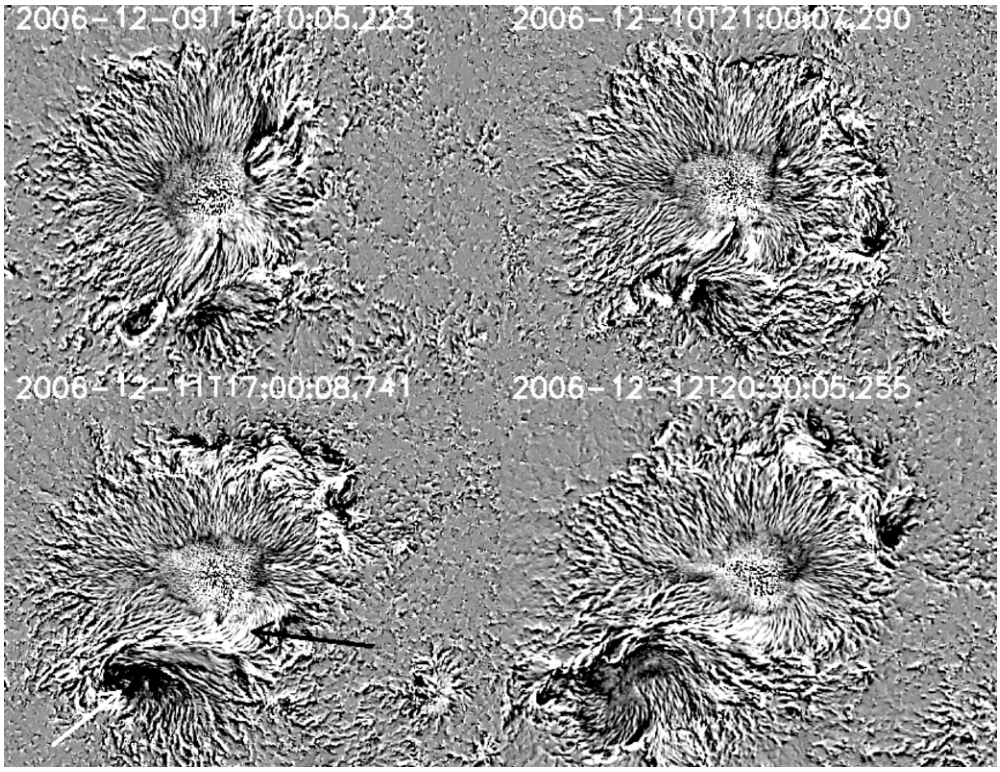

Figure 3. Maps of the vertical current density obtained at different times of the epoch. The black and white arrows in the bottom left panel show the dominant regions of the vertical current density in two different polarities. The field of view of each map is the same as in Figure 1.

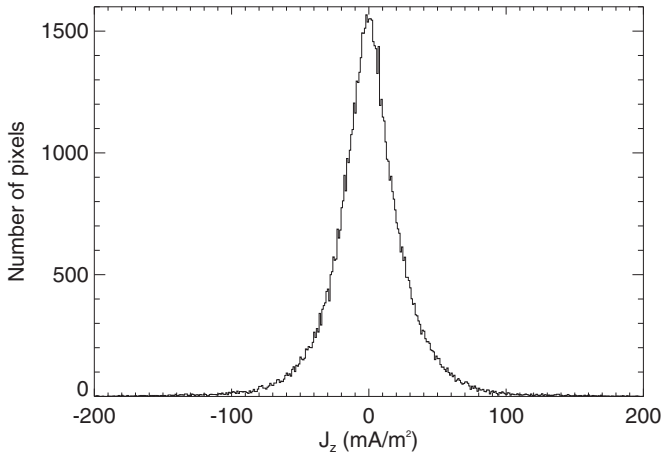

Figure 4. Histogram of the vertical current density of the full map. The values of current density extended until 200 mA m^{-2} in both the positive and negative sides.

3.2. Temporal Evolution of Net Vertical Current over the Active Region

In order to examine the temporal evolution of net vertical currents in different polarity regions, we isolated the N- and S-polarity regions by using a threshold of 50 G in the vertical magnetic field strength. We then integrated the currents for the N- and S-polarity regions separately. Figure 2 shows the net current over the N- (bottom) and S-polarity (top) regions. The net current evolution is plotted over the flux evolution to compare both of them. The negative (positive) net current is denoted by I_n (I_p), which is observed to be dominant in the N (S)-polarity region. The integrated current in each polarity is expressed in terms of amperes. We used the histogram depicted in Figure 4 to arrive at a measure of the statistical uncertainty of average vertical current density as $\delta J_z = \sigma_{J_z}/\sqrt{(N)}$ (Hagino & Sakurai 2004), where σ_{J_z} is the FWHM of the histogram and N is the number of data points. From this, we estimated the statistical uncertainty in the integrated net current as $\delta I = \sqrt{(N)} \cdot \sigma_{J_z} \cdot \Delta S$, with ΔS being the area of each pixel in m^2 (since $I = \sum_N J \cdot \Delta S$). The uncertainty in measuring the net current is shown in the top left of Figure 2. Initially, the current is small until 2006 December 10. Later, it increased linearly in both the polarities until mid-2006 December 11. The increase in the net current follows the curve of increase in flux (see Figure 2). Later, it undulates for a few hours and then starts decreasing until the end of observations. The behavior of the currents is almost the same in both polarities throughout the observations. The dashed vertical lines mark the times of the peak flux of the X3.4- and X1.3-class flares that occurred on December 13 and 14, respectively. After the X3.4-class flare, there is a decrease in net current in both polarities; however, after the X1.3-class flare the net current increased by a small amount in both polarities.

From the flux evolution map (Figure 2), it is clear that there is an increase in flux and net current until the beginning of December 12. However, the net current started to decrease after the beginning of December 12, even as the flux continued to emerge. In order to answer this puzzle, we examined the vertical current of both of the signs in each polarity region separately. Figure 5 shows the vertical currents for the S- (left) and N- (right) polarity regions. Let IN(+), IN(−), IS(+), and IS(−) denote the positive (+) and negative (−) currents in the north (N) and south (S) polarity regions. The following observations are worth noting.

1. IS(+) increased until December 12.5 by about 1.3×10^{13} A, decreased until December 13.6 by about 0.5×10^{13} A, increased again until December 14.5 by about 0.5 ×

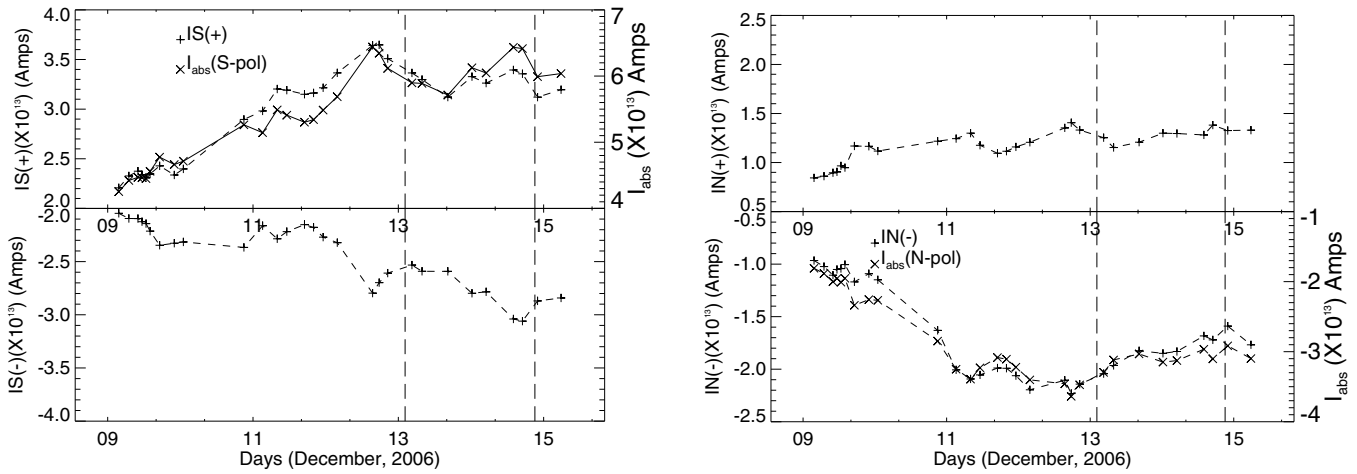

Figure 5. Left: the temporal evolution of net vertical currents in the S-polarity region (shown by + symbols). Right: the same as the left plot but for the N-polarity region. Both plots show the temporal evolution of positive and negative currents in the same polarity region. The right scale on the *Y*-axis shows I_{abs} in each of the polarities; I_{abs} is shown by × symbols.

10^{13} A, then decreased until the onset of the X1.3-class flare by about 0.2×10^{13} A, followed by a slight increase in its value. At the same time, IS(−) was almost constant at 2.2×10^{13} A with a small increase in its value until December 12.5 by about 0.5×10^{13} A. Later, it decreased until the onset of the X3.4-class flare by about 0.3×10^{13} A and then increased again until December 14.5 by about 0.6×10^{13} A, finally decreasing until the onset of the X1.3-class flare. The pattern of increase and decrease in IS(+) and IS(−) coincides well from December 11 until the onset of the X3.4-class flare. Thereafter, IS(−) increased and IS(+) decreased until the onset of the X1.3-class flare. Then, IS(−) decreased and IS(+) increased in magnitude slightly.

2. IN(−) increased until December 12.5 (with a change in the rate of increase after December 11.3) by about 1.5×10^{13} A, decreased until the onset of the X1.3-class flare by a small amount of about 0.5×10^{13} A, followed by a slight increase. On the other hand, IN(+) increased until December 12.5 (with undulations), decreased until 13.3, increased again until 14.5, then decreased until the onset of the X1.3-class flare.
3. There is a mismatch in the values of the dominant current and the non-dominant current at least by a factor of about 1.5 at all times.
4. Most importantly, the dominant current appears to follow the flux evolution in each polarity whereas the non-dominant current evolves differently.

The above observations suggest that an increase of dominant and non-dominant current could be due to both emergence and deforming flows, while a decrease in both types of currents can be either due to deforming flows or diffusion of field (we rule out the latter process in Section 4). We have noted that an increase in dominant current by and large follows the flux emergence, while increase in non-dominant current does not follow the flux evolution so closely, except in the beginning. The increase in non-dominant current results in a decrease in the net current as depicted in Figure 2. The small decrease in IS(−) and IN(+) on December 11 between 0 and 7 hr could be related to the C-class flares observed by the *Geostationary Operational Environmental Satellite* (see Figure 1(a) of Tiwari et al. 2010). The increase in the opposite current leads to a decrease in the net current in both the magnetic polarities after the beginning of December 12.

Figure 6 shows a map of the current densities which are utilized in computing the currents of different polarity regions in Figure 5. Figure 6(left) shows the map of positive and negative currents for the N-polarity region. Figure 6(right) shows the S-polarity region. The map shows that the majority of the current originates from the dominant current region, which is large in size, and the opposite current originates from the smaller-size regions, for example, the salt-and-pepper-like region in the umbra and fibril-type regions in the penumbra.

Figure 5 also shows the sum of the absolute value of the net current of both signs (I_{abs}), obtained in N- and S-polarity regions. For comparisons with the dominant current in each polarity, we have shown I_{abs} separately in IS and IN. The I_{abs} in the north polarity is shown as negative, simply to compare it with the dominant current. The plot shows that I_{abs} in the N-polarity sunspot increases with time in the beginning and reaches almost a plateau in later part of the observations. In the S-polarity region, I_{abs} increased until mid-December 12, decreased thereafter until mid-December 13 and then it increased again. I_{abs} in the S-polarity increased up to about 6×10^{13} A. There is a mismatch in the values of I_{abs} in the N- and S-polarity regions; I_{abs} is large in the S-polarity region compared to the N-polarity region. This is not unreasonable because the S-polarity carries a larger amount of flux than the N-polarity spot. The pattern of evolution of I_{abs} in both polarities follows the dominant current; however, their magnitudes are different.

4. SUMMARY AND DISCUSSION

AR NOAA 10930 is a flare-productive region and it produced several X- and M-class flares during its disk passage. The active region was associated with an emerging flux. Several morphological details of the flux emergence have already been reported (Kubo et al. 2007). In the present work, although there is a flux imbalance in the active region, the rate of flux emergence is the same in both polarities. The vector field maps showed that the transverse field in the N-polarity region was highly sheared near the PIL and there was a twisted flux rope emergence (Schrijver et al. 2008). The flux continuously increased until the end of December 12 and thereafter it leveled off until December 14, followed by a smaller bout of emergence until December

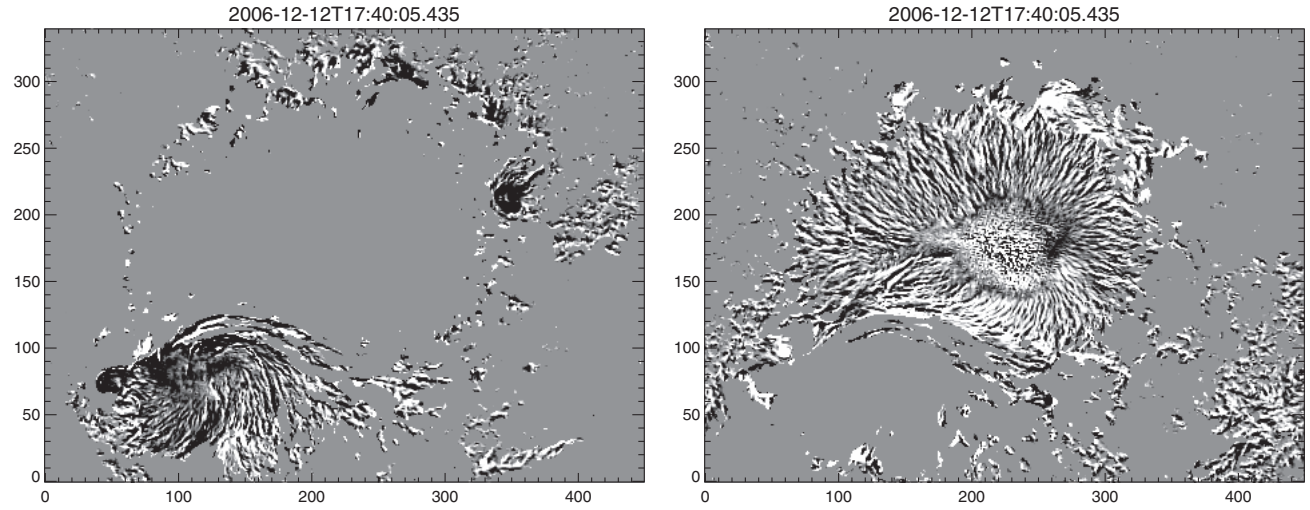

Figure 6. Maps of the vertical current density used to compute the net vertical current in the N (left) and S (right) polarity regions in the active region.

15. The net current I_n and I_p in each polarity also increased over a couple of days, and started decreasing thereafter. The decrease in the net current can be attributed to an increase in the opposite current in the same polarity region. For example, in the S-polarity region the positive current IS(+) was dominant and IS(+) increased until the end of December 12. Meanwhile, the opposite current IS(−) started increasing after beginning of December 12. A similar behavior was also found in the N-polarity region. This clearly shows that the emerging flux carries the dominant current. However, the different behavior of the non-dominant current suggests that it is largely related to the deforming motion of the flux tube but partly related to the emergence. Since the sign of current relative to the sign of flux indicates the chirality of the current, this means that the emerging flux and deforming flows produce both types of chirality of the current. If the origin of the chirality lies in the vorticity of the sub-photospheric flows that distort the magnetic field, then it shows that both signs of vorticity exist in the subsurface flows. However, note that the observed opposite current might have nothing to do with the surface or shunt current, which is required by Parker (1996) to neutralize the photospheric current for creating the field-free regions outside the sunspot.

Let us now see whether the evolution of current is related to the flares. The evolution of the current with dominant sign (IS(+) and IN(−)) in each polarity (Figure 5) is seen to decrease from December 13 to 14, the period when two X-class flares occurred. The decrease in the current of a given sign (IS(+) and IN(−)) cannot be attributed to the emergence of opposite current, as explained for the decrease of the net current (I_n and I_p). Currents can decrease either by ohmic dissipation or by deformation of the magnetic field because of plasma motion on a dynamical timescale. The timescale for this deformation is then the Alfvén travel time across the active region. Given the size of $60''$ and Alfvén speed of 10 km s^{-1} in the photosphere, the Alfvén travel time works out to be of the order of one hour. This is smaller than the cadence of the vector magnetograms. Hence, one can admit the possibility of the dynamical deformation of the field, which can then explain the decrease observed in the current. In summary, the increase in current can be attributed to emergence, while the decrease in current on timescales smaller than the diffusive time can only be attributed to the dynamical deformation of the magnetic field. It is possible that the flare could have been triggered due to such a dynamical evolution. In fact, indirect evidence for such a dynamical process associated with the December 13, X3.4-class flare, was found from the high-cadence *G*-band pictures (Gosain et al. 2009). Note that the current with the non-dominant (IS(−) and IN(+)) sign showed episodes of decrease before the onset of the X-class flares. Except IN(−), all components of the current increased for some time before each flare and then decreased. IN(−) showed no increase before the onset of the X1.3-class flare. The dynamical evolution of the magnetic field alone cannot lead to an eruption but it also needs triggering by reconnection for the same. Reconnection, in turn, requires pushing two oppositely directed magnetic field lines toward each other to a viable limit such that the magnetic field becomes discontinuous and the small-scale effects become dominant. Because of the complex dynamics of the plasma, it is unlikely that this discontinuity will form at the very beginning of the evolution phase, which explains the existence of a time delay between the onset of the evolution and the X-ray flare peak. However, it would be very difficult to predict the onset of the flare purely from a study of the photospheric magnetic field.

The emergence of dominant current (IS(+) and IN(−)) may not be a sufficient condition for the flare. It is seen at least in this active region that the flare occurs only after a significant evolution of non-dominant current. This is true for both the X3.4- and X1.3-class flares. A similar behavior is found in the case of magnetic helicity by Park et al. (2010), who observed that injection of opposite sign of helicity triggers the X3.4-class flare, which may be due to the non-dominant current. In the corona, the field is believed to be force-free. To initiate a flare, the newly emerged field lines have to be pushed against the preexisting field to produce a current sheet followed by reconnection. Therefore, there has to be some force created on the plasma to push the frozen field. Since plasma forces are not strong enough in the low-beta coronal plasma, the only force available is the Lorentz force. But the Lorentz force is possible only in a non-force-free field. It can be shown that the superposition of two force-free fields can result in a non-zero Lorentz force (see the Appendix). The necessary conditions for this are that (1) the new field must have a force-free parameter alpha which is different from that of the preexisting field and (2) the new field is not aligned with the old field. The larger the amount of the new field with the different alpha, the larger

will be the Lorentz force. This could explain our observation that the major flares occurred only after significant appearance of the oppositely directed current.

The total absolute current increased until mid-December 12. Since the larger magnitude of current implies a larger value of free magnetic energy, this behavior of the absolute current suggests that the free energy increased until mid-December 12. The current decreased from the middle of December 12, suggesting a drop in free energy. The drop in the total absolute current in the S-polarity region started well before the beginning of the X3.4-class flare, while it dropped in the N-polarity region after the flare. The decrease in the total absolute current indicates that the free energy for the flare and coronal mass ejection (CME) was supplied from this active region as suggested by Ravindra & Howard (2010), although there is a time delay between the start of the decrease in free energy as observed in the photosphere and the release of this energy to the flare and the CME. Once again, note that monitoring the free energy in the photosphere might not reveal the exact process of the delivery of this free energy to the flare and the CME. The nonlinear force-free field (NLFFF) analysis of the *Hinode* vector magnetograms by Schrijver et al. (2008) also suggests that the flares are associated with the energy carried by the currents that originate from the sub-photospheric surface.

There is yet another important result seen in these observations. We find that the net observed current within an individual spot evolves from a small value at the beginning of the flux emergence, peaks to a high value, and then diminishes to the pre-emergence values following a decrease in the rate of flux emergence. The net vertical current (I_n and I_p) in both the polarities behaved exactly opposite to each other. Even the magnitude of net current in both the polarities is almost the same throughout the observations. The temporal evolution plot of the current clearly indicates that in one polarity the current flowed into the corona and in the other polarity it returned back to the photosphere. This kind of behavior of the evolution of net vertical current has not been reported earlier. An inspection of Figure 1 shows that the transverse field was highly sheared at the PIL and not sheared at other locations of the outer penumbra of each spot. Thus, a line integral of the transverse field along a contour at the periphery of each spot would be a dominant contribution only from the PIL. Thus, the net current in the interior of this contour would be largely determined by the magnitude of the shear along the PIL. Also, the sign of the current for the contour integral around the S-polarity spot would be opposite to that around the N-polarity spot. Thus, we can attribute the symmetrical evolution of the currents in Figure 2 largely to the evolution of shear in the PIL of the active region. This is also consistent with the evolution of the mean-weighted shear angle of AR 10930 as seen in Figure 3(a) of Tiwari et al. (2010). Thus, it could well be that the contrasting results on net current obtained in earlier observations (Leka et al. 1996; Wheatland 2000; Venkatakrishnan & Tiwari 2009) are due to observations of the active regions at different stages of the flux emergence and directly related to the magnitude of the shear at the PIL. This conjecture can easily be tested with other cases of flux emergence where a time series of vector magnetograms is available. Another interesting extension of this conjecture would be that the emergence of bidirectional currents leads to a large scatter in the observed chirality of the active regions (Pevtsov et al. 1995), since the average chirality could be affected by the presence of a time-dependent contribution from a flux of opposite chirality. This points to the importance of future synoptic observations of vector magnetic fields of active regions obtained with adequate cadence to eliminate the possible effects of improper sampling of an essentially time-dependent phenomenon. Given the small dynamical timescale for field relaxation, it is essential that the spatial and spectral scanning of an active region be completed well within this timescale. From this point of view, the vector magnetograms from the Helioseismic and Magnetic Imager (Schou et al. 2010) on board the *Solar Dynamics Observatory* are eagerly awaited.

We thank the referee for useful comments that improved the presentation of the manuscript. We thank Professor Takashi Sakurai for reading a preliminary draft of the manuscript. *Hinode* is a Japanese mission developed and launched by ISAS/JAXA, with NAOJ as domestic partner and NASA and STFC (UK) as international partners. It is operated by these agencies in cooperation with ESA and the NSC (Norway).

APPENDIX

We investigate the phenomenon of flux emergence in a volume V already occupied by a magnetic field. For mathematical convenience, we assume each of the old and the new emergent magnetic fields to be in linear force-free states satisfying equations

$$\nabla \times \mathbf{B}_o = \alpha_o \mathbf{B}_o, \tag{A1}$$

and

$$\nabla \times \mathbf{B}_n = \alpha_n \mathbf{B}_n, \tag{A2}$$

where α_o and α_n are constants, $\mathbf{B}_o$ is the old magnetic field, and $\mathbf{B}_n$ is the new magnetic field. The total magnetic field in the volume V is then

$$\mathbf{B} = \mathbf{B}_o + \mathbf{B}_n. \tag{A3}$$

The total current density is obtained by taking curl on both sides of the above equation and utilizing Equations (A1) and (A2),

$$\mathbf{J} = \frac{1}{\mu}\left(\alpha_o \mathbf{B}_o + \alpha_n \mathbf{B}_n\right). \tag{A4}$$

The Lorentz force exerted by the total magnetic field $\mathbf{B}$ is calculated using Equations (A1)–(A4),

$$\mathbf{J} \times \mathbf{B} = \frac{1}{\mu}(\alpha_o - \alpha_n)\mathbf{B}_o \times \mathbf{B}_n. \tag{A5}$$

From the above expression, the superposed magnetic field is non-force-free except for the special cases of $\alpha_o = \alpha_n$, or the two fields being parallel or anti-parallel to each other. In principle, it is then possible to construct a non-force-free state by superposition of two linear force-free magnetic fields with different eigenvalues and directions. Based on the above understanding, we can think of the following plausible scenario. Let V represent an arbitrary localized volume in the corona permeated by a force-free magnetic field $\mathbf{B}_o$. The force-free approximation is justified since at coronal heights the plasma β is very small. As the new magnetic field $\mathbf{B}_n$ associated with the emergent flux attains coronal heights, it also relaxes to a force-free state because of the low β condition. If this new field

$\mathbf{B}_n$ happens to enter the localized volume V, then from the above analysis the resulting magnetic field inside V can exert a non-zero Lorentz force. We believe that this non-zero Lorentz force plays a crucial role in triggering a flare by forcing the plasma around in V so that two sub-volumes of magneto-fluid containing opposite polarity fluxes can push into each other to create a current sheet (CS) necessary for a reconnection process. In the absence of this Lorentz force, and neglecting the other forces such as plasma pressure gradient and gravity, the magneto-fluid remains in equilibrium and precludes the possibility of any CS formation and subsequent flare eruption.

REFERENCES

Aulanier, G., Démoulin, P., & Grappin, R. 2005, A&A, 430, 1067
Borrero, J. M., Lites, B. W., & Solanki, S. K. 2008, A&A, 481, L13
Chitre, S. M. 1963, MNRAS, 126, 431
Fan, Y. 2009, ApJ, 697, 1529
Gosain, S., Venkatakrishnan, P., & Tiwari, S. K. 2009, ApJ, 706, L240
Hagino, M., & Sakurai, T. 2004, PASJ, 56, 831
Hale, G. E. 1908, ApJ, 28, 315
Ichimoto, K., Lites, B., Elmore, D., et al. 2008, Sol. Phys., 249, 233
Kosugi, T., Matsuzaki, K., Sakao, T., et al. 2007, Sol. Phys., 243, 3
Kubo, M., Yokoyama, T., Katsukawa, Y., et al. 2007, PASJ, 59, S779
Leka, K. D., Barnes, G., & Crouch, A. 2009, in ASP Conf. Ser. 415, The Second Hinode Science Meeting: Beyond Discovery—Toward Understanding, ed. B. Lites, M. Cheung, T. Magara, J. Mariska, & K. Reeves (San Francisco, CA: ASP), 365
Leka, K. D., Canfield, R. C., McClymont, A. N., & van Driel-Gesztelyi, L. 1996, ApJ, 462, 547
Lim, E., Chae, J., Jing, J., Wang, H., & Weigelmann, T. 2010, ApJ, 719, 403
Lites, B. W., Elmore, D. F., Seagraves, P., & Skumanich, A. P. 1993, ApJ, 418, 928
Lites, B. W., & Skumanich, A. 1990, ApJ, 348, 747
Longcope, D. W., Fisher, G. H., & Pevtsov, A. A. 1998, ApJ, 507, 417
Longcope, D. W., & Welsch, B. T. 2000, ApJ, 545, 1089
Low, B. C. 1984, ApJ, 277, 415
Melrose, D. B. 1991, ApJ, 381, 306
Metcalf, T. R. 1994, Sol. Phys., 155, 235
Meyer, F., Schmidt, H. U., & Weiss, N. O. 1977, MNRAS, 179, 741
Park, S. H., Chae, J., Jing, J., Tan, C., & Wang, H. 2010, ApJ, 720, 1102
Parker, E. N. 1979, Cosmical Magnetic Fields: Their Origin and Their Activity (Oxford: Clarendon)
Parker, E. N. 1996, ApJ, 471, 485
Pevtsov, A. A., Canfield, R. C., & Metcalf, T. R. 1995, ApJ, 440, L109
Ravindra, B., & Howard, T. A. 2010, Bull. Astron. Soc. India, 38, 147
Schou, J., Borrero, J. M., Norton, A. A., et al. 2010, Sol. Phys.
Schrijver, C. J., DeRosa, M. L., Metcalf, T., et al. 2008, ApJ, 675, 1637
Skumanich, A., & Lites, B. W. 1987, ApJ, 322, 473
Su, J. T., Sakurai, T., Suematsu, Y., Hagino, M., & Liu, Y. 2009, ApJ, 697, 103
Suematsu, Y., Tsuneta, S., Ichimoto, K., et al. 2008, Sol. Phys., 249, 197
Tiwari, S. K., Venkatakrishnan, P., & Gosain, S. 2010, ApJ, 721, 622
Tiwari, S. K., Venkatakrishnan, P., & Sankarasubramanian, K. 2009, ApJ, 702, 133
Tsuneta, S., Ichimoto, K., Katsukawa, Y., et al. 2008, Sol. Phys., 249, 167
Venkatakrishnan, P., Hagyard, M. J., & Hathaway, D. H. 1989, Sol. Phys., 122, 215
Venkatakrishnan, P., & Tiwari, S. K. 2009, ApJ, 706, 114
Venkatakrishnan, P., & Tiwari, S. K. 2010, A&A, 516, L5
Wang, H., Jing, J., Tan, C., Weigelmann, T., & Kubo, M. 2008, ApJ, 687, 658
Wheatland, M. S. 2000, ApJ, 532, 616